AIP Journal of Applied Physics

Electrical characterization of defects introduced in n-Ge during electron beam deposition or exposure

S. M. M. Coelho, F. D. Auret, P. J. Janse van Rensburg, and J. M. Nel

Citation: Journal of Applied Physics **114**, 173708 (2013); doi: 10.1063/1.4828999
View online: http://dx.doi.org/10.1063/1.4828999
View Table of Contents: http://scitation.aip.org/content/aip/journal/jap/114/17?ver=pdfcov
Published by the AIP Publishing

Articles you may be interested in

Electron and hole deep levels related to Sb-mediated Ge quantum dots embedded in n-type Si, studied by deep level transient spectroscopy
Appl. Phys. Lett. **102**, 232106 (2013); 10.1063/1.4809595

Characterization of the E(0.31) defect introduced in bulk n-Ge by H or He plasma exposure
J. Appl. Phys. **111**, 044511 (2012); 10.1063/1.3687426

Electrical characterization of defects introduced in n -type Ge during indium implantation
Appl. Phys. Lett. **89**, 152123 (2006); 10.1063/1.2360922

Electrical characterization of defects introduced during electron beam deposition of Pd Schottky contacts on n -type Ge
Appl. Phys. Lett. **88**, 242110 (2006); 10.1063/1.2213203

Electrical characterization of defects introduced in p- Si 1x Ge x during electron-beam deposition of Sc Schottky barrier diodes
Appl. Phys. Lett. **72**, 1069 (1998); 10.1063/1.120967

Re-register for Table of Content Alerts

Create a profile.
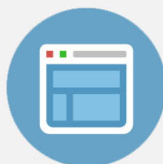
Sign up today!

[This article is copyrighted as indicated in the article. Reuse of AIP content is subject to the terms at: http://scitation.aip.org/termsconditions. Downloaded to] IP: 137.215.6.53 On: Tue, 22 Apr 2014 06:13:18

JOURNAL OF APPLIED PHYSICS **114**, 173708 (2013)

Electrical characterization of defects introduced in n-Ge during electron beam deposition or exposure

S. M. M. Coelho, F. D. Auret, P. J. Janse van Rensburg, and J. M. Nel
Department of Physics, University of Pretoria, Private Bag X20, Hatfield, 0028, South Africa

(Received 14 September 2013; accepted 18 October 2013; published online 6 November 2013)

Schottky barrier diodes prepared by electron beam deposition (EBD) on Sb-doped n-type Ge were characterized using deep level transient spectroscopy (DLTS). Pt EBD diodes manufactured with forming gas in the chamber had two defects, $E_{0.28}$ and $E_{0.31}$, which were not previously observed after EBD. By shielding the samples mechanically during EBD, superior diodes were produced with no measureable deep levels, establishing that energetic ions created in the electron beam path were responsible for the majority of defects observed in the unshielded sample. Ge samples that were first exposed to the conditions of EBD, *without metal deposition* (called electron beam exposure herein), introduced a number of new defects not seen after EBD with only the E-center being common to both processes. Substantial differences were noted when these DLTS spectra were compared to those obtained using diodes irradiated by MeV electrons or alpha particles indicating that very different defect creation mechanisms are at play when too little energy is available to form Frenkel pairs. These observations suggest that when EBD ions and energetic particles collide with the sample surface, inducing intrinsic non-localised lattice excitations, they modify defects deeper in the semiconductor thus rendering them observable. © *2013 AIP Publishing LLC*. [http://dx.doi.org/10.1063/1.4828999]

I. INTRODUCTION

In the microelectronics and photovoltaic industries, metallization is a necessary process. Deposition of high melting point metals and the ability to accurately control the deposition rate make electron beam deposition (EBD) an ideal choice that is widely accepted in industry.[1] Metallization processes, including EBD, introduce defects at and close to the metal-semiconductor junction that influence device performance[2] and alter a contact's barrier height.[3] The defects that are responsible for this device modification are introduced when energetic particles impinge on the semiconductor surface causing lattice damage such as vacancies or interstitials.[4]

Here, we report on the defects introduced in bulk-grown, antimony doped, n-type germanium during EBD of Pt while mechanically shielding the sample from the direct path of energetic particles that originate in the electron beam (EB). The availability of ultra-pure germanium made it an ideal candidate for this study.[5] The effect of vacuum quality on defect introduction is also noted. Furthermore, exposing samples to EB conditions, *without metal deposition* [termed EB exposure (EBE) herein] prior to metal deposition by resistive evaporation (RE) was used to illustrate fundamental differences between the defects introduced. These diodes exhibited defects not seen after EBD, RF sputter deposition, or MeV electron irradiation.

II. EXPERIMENTAL PROCEDURE

Umicore bulk grown Ge doped with Sb to a level of $1 \times 10^{15}\,\mathrm{cm}^{-3}$ was degreased in successive 5 min ultrasonic baths of trichloroethylene, isopropanol, and methanol and then etched in a solution of 5:1, H_2O:H_2O_2 (30%) for 1 min. Au/Sb (0.6%) alloy was evaporated resistively onto the back surface and subsequently annealed at 350 °C for 10 min, lowering the contact resistance, thus forming an ohmic contact. This cleaning procedure was repeated before samples were again loaded into a vacuum chamber and pumped to a pressure below 10^{-6} mbar, where metal was deposited onto the front surface through a metal contact mask, typically yielding eight Schottky barrier diodes with a diameter of 0.6 mm. All samples were cut from the same wafer.

Vacuum pumping was carried out by a dry pump in series with a turbomolecular pump and to lower the H_2 concentration. Ti and Pd were evaporated in the chamber with the sample rotated away from the evaporation source. While the pre-deposition vacuum was typically 5×10^{-7} mbar, this soon went up to approximately 3×10^{-6} mbar during the evaporation. As the vacuum conditions vary greatly during EBD, forming gas H15 with a composition of N_2:H_2 of 85%:15% by volume was also used to raise the pressure in the vacuum chamber to 10^{-4} mbar and kept constant during processing of select samples. EBE of samples and EBD of contacts were accomplished using a 10 kV source (MDC model e-Vap 10CVS) with the samples positioned 50 cm above the crucible. EBD samples were turned away from the target until such time as the evaporation rate had stabilised and then deposition could proceed. Shielding of samples from energetic particles originating in the EB path was carried out using 1 mm thick stainless steel plates, shield 1 shielding from particles on a direct trajectory from the electron beam path to the sample, and shield 2 placed to shield from energetic particles reflected off the chamber wall, shown diagrammatically in Ref. 6. A beam current of 100 mA was required to evaporate Pt at a rate of $0.02\,\mathrm{nm \cdot s^{-1}}$ resulting in 50 nm thick Schottky barrier diodes in an evaporation of approximately 40 min. During EBE, *without metal deposition*, the samples were exposed for 50 min; while the beam heated a tungsten source using a beam current of

 © 2013 AIP Publishing LLC

[This article is copyrighted as indicated in the article. Reuse of AIP content is subject to the terms at: http://scitation.aip.org/termsconditions. Downloaded to] IP: 137.215.6.53 On: Tue, 22 Apr 2014 06:13:18

100 mA, this current being insufficient to evaporate W, thus exposing the samples to EB conditions comparable to those experienced during deposition. Platinum with its high work function was chosen as a moderately high beam current was required to evaporate it and the same beam current was sufficient to introduce defects during the EBE process, albeit in low concentrations. Palladium diodes were used for all the other samples prepared for this study as it can be evaporated resistively, a process that is known to not introduce defects in concentrations measurable by deep level transient spectroscopy (DLTS).

After contact fabrication, current-voltage (IV) and capacitance-voltage (CV) measurements were performed to determine diode quality and the free carrier concentration of the Ge samples, found to be $1.3 \times 10^{15}\,cm^{-3}$. Conventional DLTS and Laplace DLTS (L-DLTS)[7] were then used to study the defects introduced by EBD and EBE. Comparing these defects to those introduced by high energy electron irradiation from a strontium-90 (Sr-90) source,[8] α-particle irradiation from an americium 241 (Am-241) radio-nuclide, low energy RF sputter etching, and both capacitively and inductively coupled plasma (ICP) etching, allowed us to identify defects that were only observed after the 10 kV EBD or the EBE process. This Sr-90 source has an effective fluence rate of electrons with energies above 200 keV of 10^9 electrons $cm^{-2}\,s^{-1}$, and the Am-241 foil has an effective fluence for α-particles of 7×10^6 α-particles cm^{-2} s^{-1} with energies of 5.4 MeV. Samples were exposed to these sources for 20 h and 3 h, respectively. DLTS spectra obtained for these samples were then compared to those obtained from 100 nm thick Pd diodes prepared by EBD. Furthermore, L-DLTS was used to split DLTS signals of defects with energies that were too closely spaced for conventional DLTS to resolve. DLTS peak amplitudes can be converted to deep level concentration, N_T, as $\frac{N_T}{N_D} \approx \frac{2\Delta C}{C}$, where N_D is the concentration of shallow impurities, ΔC is the DLTS peak height, and C is the junction capacitance. The samples prepared for this study had similar measured capacitances at room temperature that were reduced by, at most, 5 pF as the samples were cooled to 25 K making it easy to compare relative defect concentrations by comparing peak heights of DLTS spectra directly.

III. RESULTS AND DISCUSSIONS

A. High energy particle irradiation

A mini review of the literature with regards to the defects observed after 2 MeV proton irradiation is available,[9] but as the defects introduced during EBD of Schottky barrier diodes will be compared with those observed after high energy (MeV) electron irradiation and α-particle irradiation, it is instructive to first discuss the possible mechanisms by which defects are introduced in single crystal germanium. Grown-in electrically active defects were not present in measurable quantities in these samples, that is, with concentrations above $10^{11}\,cm^{-3}$ (control, Figure 1), and thus only defects resulting from collisions of energetic particles with the crystal will be considered. The first type of defect is created when an incident particle imparts enough energy E_d to a lattice atom to displace it forming a stable vacancy-interstitial defect known as a

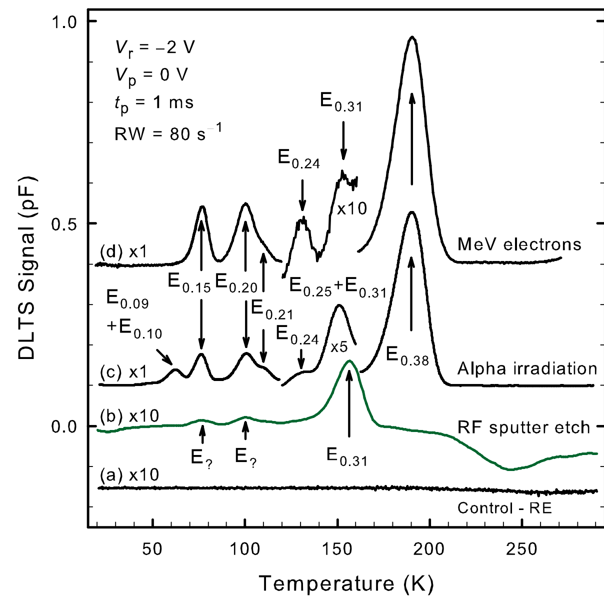

FIG. 1. DLTS spectra of n-Ge resistively evaporated Pd diodes that were (a) not irradiated (control), (b) RF sputter cleaned in a plasma with 300 eV Ar ions, (c) irradiated with α-particles from an Am-123 source, and (d) MeV electron-irradiated by a Sr-90 source. All spectra were recorded with a rate window of $80\,s^{-1}$, pulse width of 1 ms, quiescent reverse bias of −2 V, and a filling pulse amplitude 2 V. Plots have been offset along the y-axis for clarity.

Frenkel pair. Divacancies, trivacancies, and vacancy clusters can form when vacancies combine. In germanium, experimentally obtained values for E_d vary from 15 to 30 eV and Holmstrom *et al.* concluded that their calculated value of 11.5 eV as a global minimum is in fair agreement with experiment.[10] For the specific case of electron irradiation, applying conservation of momentum while neglecting relativity, an incident electron is required to have a threshold energy E_d of 380 keV to transfer the 11.5 eV required to displace a Ge atom from its lattice position assuming a perfect elastic collision. A two-step process has been suggested involving a light impurity atom, like hydrogen, as a more efficient energy transfer mechanism, and this was discussed in some detail by Chen and MacKay.[4] At that time, they concluded that the defects they observed could only have been generated by sub-threshold energy electrons in germanium crystals grown in hydrogen as they observed damage after 40 keV irradiations, establishing this as the minimum required to generate defects. Using an intermediate light atom would have raised the energy transferred by a small fraction, but this alone would not be enough to account for their observations. Much later, Mooney and Bourgoin concluded that intrinsic point defects are not created by sub-threshold irradiation[11] as previous evidence of point defect creation failed to take into account defects caused by impurities or the effect of surface states on measurements. They reported that MeV electron irradiation introduced vacancy and divacancy defects in Ge, but their conclusions with regard to sub-threshold electron irradiation are in contradiction to subsequent reports of the E-center, for example, the vacancy-Sb complex in Sb doped Ge, being introduced by EBD in Ge (Ref. 12) and Si.[6] When considered in context, the observations of Mooney and Bourgoin support the theory, and the conclusions drawn from their observations

[This article is copyrighted as indicated in the article. Reuse of AIP content is subject to the terms at: http://scitation.aip.org/termsconditions. Downloaded to] IP: 137.215.6.53 On: Tue, 22 Apr 2014 06:13:18

are valid as their DLTS measurement parameters would not have observed defects that are only found close to the metal-semiconductor interface, in small concentrations.

Impurity atoms may be present in the semiconductor or they can also be introduced during processing, intentionally (implantation), or unintentionally, when accelerated particles penetrate the semiconductor occasionally moving deeper into the crystal aided by diffusion processes. These impurity atoms may distort the crystal lattice but are also known to attach themselves to dangling bonds, thus passivating shallow donors, shallow acceptors, as well as defects with levels deep in the bandgap.[13,14] The complexes formed by hydrogen with germanium fall within this class of defect, and while this has been studied extensively in silicon,[13] very few similar studies have been undertaken in germanium.[15] The properties of hydrogen in germanium were not expected to differ vastly from silicon and yet some as yet unexplained differences have been observed.[16] Hydrogen is readily incorporated into Ge in concentrations of 10^{14} to $10^{15}\,cm^{-3}$ during growth,[17] but attempts to passivate defects by H implantation have been unsuccessful.[16] Using density functional theory calculations, VH_n (n = 1, 2, 3, or 4) in Ge was predicted to have energy levels in the bandgap[18] for n = 1 and n = 3. If the hydrogen is removed, then the vacancy that results is mobile at room temperature and can form a complex with other impurities, the most likely one of which is the E-center. The Ge-Ge and Ge-H bond strengths are 1.93 and 3.59 eV, respectively,[19,20] but as only one bond is being broken at a time in the Ge-H case and as H is much lighter than Ge, a 10 keV electron can transfer as much as 24 eV to a H atom, more than enough to break the Ge-H bond. Calculating the maximum energy in which an incident electron is able to transfer in an elastic collision yields the surprising result that it is required to have energy as much as 300 times lower to displace H compared to the 380 keV required to displace Ge from the lattice. This argument also holds for H in the Si lattice although the energy difference ratio will be lower.

In Figure 1, DLTS spectra from MeV electron irradiated,[12] alpha particle irradiated,[21] and 300 eV RF sputter etched Ge are plotted for comparison purposes. A control sample prepared by RE demonstrates that no defects were present in the Ge samples in measurable quantities before irradiation, i.e., above $10^{10}\,cm^{-3}$. The MeV electron and alpha irradiated samples are very similar except that the alpha irradiated Ge had three additional defects, $E_{0.09}$, $E_{0.10}$, and $E_{0.25}$, where E refers to an electron trap and the subscript 0.10 refers to an energy level that is 0.10 eV below the conduction band. A similar convention will apply for hole traps except that $H_{0.31}$ will indicate a hole trap with an energy 0.31 eV above the valence band. The RF sputter etched sample was exposed to energetic argon ions with a maximum energy of 300 eV for 10 min, and this treatment yielded a spectrum that only had one defect $E_{0.31}$ with a concentration high enough to be measured using L-DLTS. From the Arrhenius plot in Figure 3, we deduce that this defect is different to a defect of similar energy introduced by MeV electron and alpha irradiation but that this defect was previously observed after ICP etching with argon[22] and H-passivation.[23] ICP etching was carried out using argon ions with energies less than 100 eV and did not introduce the defects that RF plasma etching introduced at the positions of the $E_{0.15}$ and $E_{0.20}$ defects, although these were present in very low concentrations. A more appropriate comparison between RF sputtering and ICP sputtering was not possible as 300 V was the lowest accelerating voltage that could sustain a plasma in the Leybold Z400 sputter system. Nyamere *et al.* reported on the defects introduced by 3 keV Ar sputtering of Ge after which $E_{0.38}$ and an additional seven hole traps were observed, some of these defects only being observed after annealing.[24] The defects observed after 300 eV RF sputtering or ICP etching were not observed by Nyamere *et al.* suggesting that $E_{0.31}$ is introduced when the Ar ion accelerating voltage is low and not necessarily dependant on the plasma being capacitively or inductively coupled. ICP etching with 4 eV Ar ions still introduces $E_{0.31}$ but as ions with lower energy were not attempted, 4 eV was not established as the lowest energy that is required to introduce this defect. Hydrogen,[23] neon, and oxygen plasmas also introduced the same defect, without additional defects being observed.

B. Electron beam deposition

EBD introduces a number of defects in Ge that have been reported before and are summarized in Table I.[12,25,26] Comparing DLTS spectra in the literature, it is evident that while similarities exist between EBD spectra of different metals evaporated onto Ge, there are also differences, both in the defects observed and the relative heights of these peaks. When EBD diodes are compared to MeV electron and alpha particle irradiated diodes, then only the E-center, $E_{0.38}$, is common to all three processes. $H_{0.30}$ (V-Sb related) is introduced by EBD and MeV electron irradiation. The $E_{0.10}$ defect introduced during α-particle irradiation has the same energy as a defect introduced during EBD, but it is unlikely that this defect is common to these two processes as there is a small difference in the Arrhenius plots of these defects. Also, the absence of this defect after MeV electron irradiation, a process using energetic particles with energy between EBD and α-particle irradiation, suggests that $E_{0.10}$ (α) and $E_{0.10}$ (EBD) are different defects. It is possible that $E_{0.10}$ (EBD) and $E_{0.09}$ (α) are the same defect, but in the absence of annealing data, we cannot be certain. Not all α-particle irradiation defects were reported on previously, and thus $E_{0.09}$, $E_{0.24}$, $E_{0.25}$, $E_{0.31}$, and $H_{0.31}$ have been included here for completeness.

During the coating process, samples in EBD chambers are bombarded by both negatively and positively charged particles as verified by measuring the current flowing through the sample holder during deposition. A 10 kV potential was applied to accelerate electrons emitted by the EB filament, and modern EBD systems are carefully designed to shield this filament from the samples being coated. The filament is positioned below the crucible, requiring that the electron beam be manipulated by a magnetic field to follow a circular path towards the crucible through an angle of 270°. The magnetic field will focus electrons onto the target, but positive ions generated near the filament will follow a path away from the crucible with a much larger radius due to their larger mass. This arrangement makes it highly improbable

[This article is copyrighted as indicated in the article. Reuse of AIP content is subject to the terms at: http://scitation.aip.org/termsconditions. Downloaded to] IP: 137.215.6.53 On: Tue, 22 Apr 2014 06:13:18

TABLE I. Defects observed in Ge after various processing or irradiation techniques. "*" shows experimental data in this report.

Process	Defect label	E_T (eV)	σ_a ($\times 10^{-15}$ cm^2)	T_{80}[a] (K)	Similar defects/defect ID/Ref.
EBD	$E_{0.10}$	$E_C - 0.10$	0.37	65	$E_{0.10}$ (Ref. 12)
	$E_{0.13}$	$E_C - 0.13$	0.19	85	$E_{0.13}$ (Ref. 12)
	$E_{0.23}$	$E_C - 0.23$	34	116	$E_{0.13}$ (Ref. 12)
	$E_{0.38}$	$E_C - 0.38$	10	191	$E_{0.37}$,[9] E_{377},[30] $E_{0.38}$,[12,25] V-Sb (–/-) (Refs. 9 and 30)
	$H_{0.09}$	$E_V + 0.09$	210	47	$H_{0.09}$,[12] V-Sb (0/+) (Ref. 31)
	$H_{0.15}$	$E_V + 0.15$	71	82	$H_{0.15}$ (Ref. 12)
	$H_{0.18}$	$E_V + 0.18$	35	97	$H_{0.18}$ (Ref. 12)
	$H_{0.27}$	$E_V + 0.27$	240	133	$H_{0.27}$,[12] H_{270} (Ref. 30)
	$H_{0.30}$	$E_V + 0.30$	620	141	H_{307},[30] $H_{0.30}$,[9] V-Sb (-/0) (Ref. 30)
	$H_{0.29}$	$E_V + 0.29$	1.3	176	$H_{0.29}$ (Ref. 25)
EBD (f/gas)	$E_{0.28}$	$E_C - 0.28$	11	153	*
	$E_{0.31}$	$E_C - 0.31$	9.0	163	*
EBE	$E_{0.16}$	$E_C - 0.16$	320	77	*
	$E_{0.22}$	$E_C - 0.22$	515	101	*
	$E'_{0.22}$	$E_C - 0.22$	69	108	*
	$E_{0.33}$	$E_C - 0.33$	246	152	*
	$E_{0.37}$	$E_C - 0.37$	35.4	182	*, $E_{0.37}$ (Ref. 12)
	$E_{0.38}$	$E_C - 0.38$	13.8	192	*, E_{377},[30] $E_{0.38}$,[12,25] V-Sb (–/-) (Ref. 30)
	$H'_{0.15}$	$E_V + 0.15$	65	86	*
	$H_{0.22}$	$E_V + 0.22$	1960	106	*
	$H_{0.26}$	$E_V + 0.26$	89	139	*
	$H_{0.34}$	$E_V + 0.34$	172	171	*
ICP	$E_{0.31}$	$E_C - 0.31$	10	157	$E_{0.31}$,[22] $E(0.30)$ (Ref. 23)
Sputter etch	$E_{0.31}$	$E_C - 0.31$	10	157	* (~300 eV Ar), $E_{0.31}$ (Refs. 22 and 23)
Sputter deposition	$ES_{0.14}$	$E_C - 0.14$	5.5	78	$ES_{0.14}$,[32] $E_{0.13}$, Sb and I related[9]
	$ES_{0.20}$	$E_C - 0.20$	37	100	$ES_{0.20}$,[32] $E_{0.19}$, Sb and I related[9]
	$ES_{0.21}$	$E_C - 0.21$	20	109	$ES_{0.21}$,[32] $E_{0.21}$ (Ref. 9)
	$ES_{0.24}$	$E_C - 0.24$	3.3	131	$ES_{0.24}$,[32] $E_{0.23}$ (Ref. 9)
	$ES_{0.31}$	$E_C - 0.31$	15	151	$ES_{0.31}$,[32] $E_{0.29}$,[9] Divacancy?[9]
MeV electron irradiation	$E_{0.15}$	$E_C - 0.15$	50	77	$E_{0.15}$ (Ref. 12)
	$E_{0.20}$	$E_C - 0.20$	14	100	$E_{0.20}$,[12] $E_{0.19}$, Sb and I related[9]
	$E_{0.21}$	$E_C - 0.21$	36	109	$E_{0.21}$,[12] $E_{0.21}$, Sb related?[9]
	$E_{0.24}$	$E_C - 0.24$	2.5	131	$E_{0.24}$,[12] E(0.23) (Ref. 33)
	$E_{0.31}$	$E_C - 0.31$	50	151	$E_{0.31}$ (Ref. 12)
	$E_{0.37}$	$E_C - 0.37$	29	181	$E_{0.37}$ (Ref. 12)
	$E_{0.38}$	$E_C - 0.38$	11	191	E_{377},[30] $E_{0.37}$,[9] V-Sb (–/-) (Ref. 30)
	$H_{0.30}$	$E_V + 0.30$	366	142	H_{307},[30] $H_{0.30}$,[9] V-Sb (-/0) (Ref. 30)
Alpha irradiation	$E_{0.09}$	$E_C - 0.09$	0.66	63	*, $E_{0.10}$?[12]
	$E_{0.10}$	$E_C - 0.10$	9.2	59	$E_{0.10}$ (Ref. 21)
	$E_{0.15}$	$E_C - 0.15$	62	76	$E_{0.15}$ (Ref. 21)
	$E_{0.20}$	$E_C - 0.20$	78	99	$E_{0.20}$,[21] $E_{0.19}$, Sb and I related[9]
	$E_{0.21}$	$E_C - 0.21$	29	109	$E_{0.21}$,[21] $E_{0.21}$, Sb related?[9]
	$E_{0.24}$	$E_C - 0.24$	14.5	130	*, $E_{0.23}$ (Ref. 9)
	$E_{0.25}$	$E_C - 0.25$	0.37	149	*
	$E_{0.31}$	$E_C - 0.31$	98	151	*, $E_{0.30}$ (Ref. 9)
	$E_{0.38}$	$E_C - 0.38$	13	190	$E_{0.38}$,[21] V-Sb (–/-) (Ref. 30)
	$H_{0.31}$	$E_v + 0.31$	1000	142	*, $H_{0.31}$,[21] $H_{0.30}$,[9] H_{307}, V-Sb (-/0) (Ref. 30)

[a]Peak temperature at a rate window of 80 s^{-1}.

that 10 keV ions originated near the filament will arrive at the sample in sufficient numbers to cause measurable defects. The same cannot be said for ions that are generated in the electron beam path when 10 keV electrons collide with residual gas atoms in the vacuum. Slow moving, heavy atoms in the beam path have a greater probability of colliding with energetic electrons, but even for a fast moving atom like hydrogen, the probability of a collision is above one if it travels across a typical electron beam required to melt Pt. The number of energetic particles that collide with a sample is dependent on many parameters, including the EB current, vacuum pressure, residual gas composition, beam diameter, sample distance, and deposition time, and most parameters that are not readily controlled. Shielding the sample during deposition is easily implemented, and the spectra in Figure 2 illustrate that mechanical shielding of the sample can have an impact on the number of defects introduced during EBD. All the diodes were prepared in the same vacuum system

[This article is copyrighted as indicated in the article. Reuse of AIP content is subject to the terms at: http://scitation.aip.org/termsconditions. Downloaded to] IP: 137.215.6.53 On: Tue, 22 Apr 2014 06:13:18

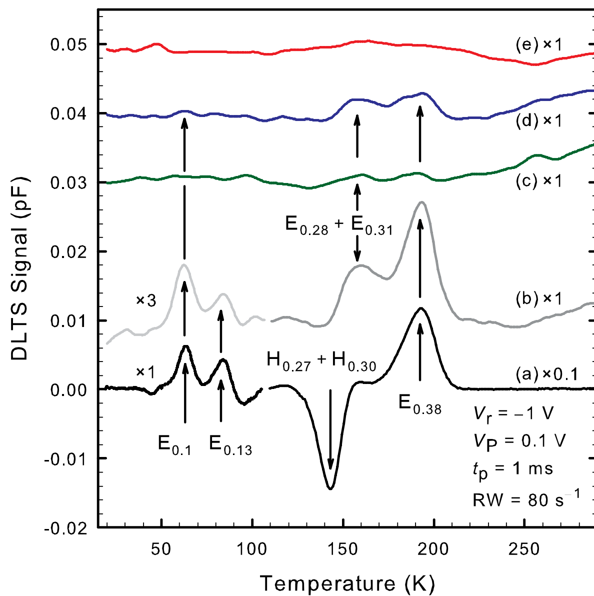

FIG. 2. DLTS spectra of EBD Pt SBDs (Schottky barrier diodes) to demonstrate the effects of shielding on defect concentration: (a) no shielding and standard vacuum conditions. For curves (b)–(d), the chamber was backfilled with forming gas to 10^{-4} mbar where (b) no shielding was applied, (c) one shield applied to shield from direct particles, and (d) two shields to additionally shield from particles reflected off the chamber wall. Curve (e) diode was deposited in a superior vacuum with two shields in place.

that was initially pumped down to 10^{-6} mbar. An oil-filled rotary vane pump was used only when depositing Pt for the diode of plot (a), whereas all other diodes were prepared after the chamber was evacuated using a dry pump. Dry pumping minimizes the potential for hydrocarbons to contaminate the deposition chamber. As the chamber heats up during EBD, it is often a problem that the pressure increases sharply

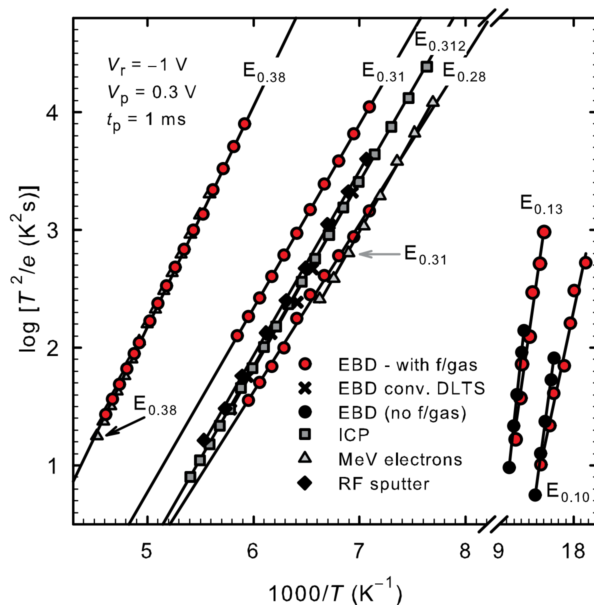

FIG. 3. L-DLTS Arrhenius plots of electron trap defects observed after Pt EBD in forming gas (filled circles). Where these defects have also been observed after MeV electron irradiation, argon RF sputter etching, and argon ICP, these plots have also been included. The defect peak plot (crosses) obtained by conventional DLTS was then split using L-DLTS into $E_{0.28}$ and $E_{0.31}$.

during deposition. During the deposition of diode (a), the vacuum pressure increased to approximately 10^{-4} mbar, whereas during the EBD of diode (e), the pressure only increased to 3×10^{-6} mbar. All other diodes were prepared at a pressure of 10^{-4} mbar that was kept constant by adjusting the flow of forming gas into the chamber.

Seven defects were introduced during EBD of Pt when there were neither shields used nor forming gas introduced in the chamber (Figure 2, plot (a)). The hole traps, $H_{0.27}$, $H_{0.29}$, and $H_{0.30}$, were only observed in this sample. Once forming gas was introduced into the chamber, two electron traps, $E_{0.28}$ and $E_{0.31}$, were introduced that were not previously seen after EBD. The E-center ($E_{0.38}$) was common to all samples except the sample prepared in a superior vacuum with two shields in place as this sample did not have any defects with a concentration high enough to measure. As the DLTS graph peak heights are proportional to the defect concentrations, the smaller peak heights in Figure 2 of the shielded samples demonstrate the effectiveness of shielding in lowering defect concentration. All the defects observed after EBD in forming gas have been plotted in the Arrhenius plot of Figure 3, and the defects that are similar to defects observed after ICP, MeV electron irradiation, and RF sputtering have also been included. The defect concentrations of the $E_{0.10}$ and $E_{0.13}$ defects were too small to provide an accurate energy level determination, and the energies displayed were calculated using data from the EBD sample deposited without using forming gas (Figure 2, plot (a)). Using conventional DLTS, the $E_{0.31}$ defect (crosses in Figure 3) seemed identical to a defect observed after ICP etching, and this ICP defect is labelled $E_{0.312}$ for clarity. L-DLTS of this peak splits this single peak into two peaks with energies $E_{0.28}$ and $E_{0.31}$ that were only observed once forming gas was introduced. Three electron traps, all with enthalpy of approximately 0.31 eV, have been plotted in Figure 3. The Arrhenius plots of these defects, although similar, do not line up indicating that they are different defects. At present, the best evidence that these are unique defects observed after different processing techniques is found by comparing the respective peak temperatures of their 80 s^{-1} rate window DLTS spectra (Table I). Multiple scans that took approximately 20 h were performed at each temperature to improve the signal to noise ratio thus making it possible to extract useful data. This serves as a good example of the value of L-DLTS, both in resolving very small signals and in splitting a peak consisting of two closely spaced energy levels.

A summary of the IV and CV data collected for these diodes appears in Table II. All EBD diodes manufactured with shields in place had superior characteristics as their ideality was less than 1.06 and the reverse bias current measured with 1 V applied was below 8×10^{-4} A cm^{-2}. Diodes manufactured with a good vacuum and two shields had ideality closest to one (below 1.02 in some instances) and the lowest reverse bias current of all diodes that have been fabricated to date by this group. IV plots in Figure 4 compare such a diode (crosses) with diodes manufactured without shielding. By comparing the best seven out of eight diodes manufactured for each EBD scheme, the diodes evaporated in a superior vacuum with two shields in place had the

[This article is copyrighted as indicated in the article. Reuse of AIP content is subject to the terms at: http://scitation.aip.org/termsconditions. Downloaded to] IP: 137.215.6.53 On: Tue, 22 Apr 2014 06:13:18

TABLE II. EBD Pt diodes fabricated under different vacuum and system configuration conditions. F/gas refers to forming gas with a ratio of 85%:15%, nitrogen: hydrogen.

Pt diodes	Ideality—best diode	I at 1 V reverse bias ($A\cdot cm^{-2}$)	I average of 7 diodes (Std. deviation) ($A\cdot cm^{-2}$) at −1 V	Schottky barrier height—IV (eV)	Schottky barrier height—CV (eV)
Unshielded	1.12	1.24×10^{-3}	1.42×10^{-3} (8.58×10^{-4})	0.56 ± 0.04	0.50 ± 0.03
Unshielded and f/gas	1.05	7.78×10^{-4}	6.65×10^{-3} (5.76×10^{-3})	0.55 ± 0.04	0.51 ± 0.03
Shield 1 and f/gas	1.04	2.90×10^{-4}	6.20×10^{-3} (7.30×10^{-3})	0.58 ± 0.04	0.50 ± 0.03
Shield 1 and 2, f/gas	1.03	3.47×10^{-4}	2.03×10^{-2} (2.88×10^{-2})	0.58 ± 0.04	0.51 ± 0.03
Shield 1 and 2	1.02	2.48×10^{-4}	3.47×10^{-4} (2.05×10^{-4})	0.59 ± 0.04	0.51 ± 0.03

lowest reverse bias current at 1 V coinciding with the lowest standard deviation.

The most significant observation from this series of EBD samples is that the DLTS peak heights consistently decreased in height with the application of mechanical shields (Figure 2, plots (c) and (d)) with a further reduction in concentrations to below the measurement threshold when the vacuum improved (Figure 2, plot (e)). The small fluctuations in plot (e) of Figure 2 are indicative of surface states that may be damage caused by a small number of light ions deflected by the EB system magnetic field to follow a curved trajectory around shield 1. The shields were positioned to minimize the number of energetic ions that reached the samples and were unable to eliminate bombardment from electrons being reflected off the metal target. This was confirmed by measuring the current at the sample position with a Faraday cup, such negative current is increased by an order of magnitude as the target surface melted. While 10 keV electrons have enough energy to damage our Ge samples, they were not the primary cause of the defects observed. Rather the energetic ions that are always present during EBD, colliding with the semiconductor or the metal surface, introduced the observed defects. As the semiconductor surface is rapidly coated with metal, most of the EBD-induced damage must be introduced by collisions of low energy ions, atoms, or molecules with the metal layer, while this metal layer grows in thickness.

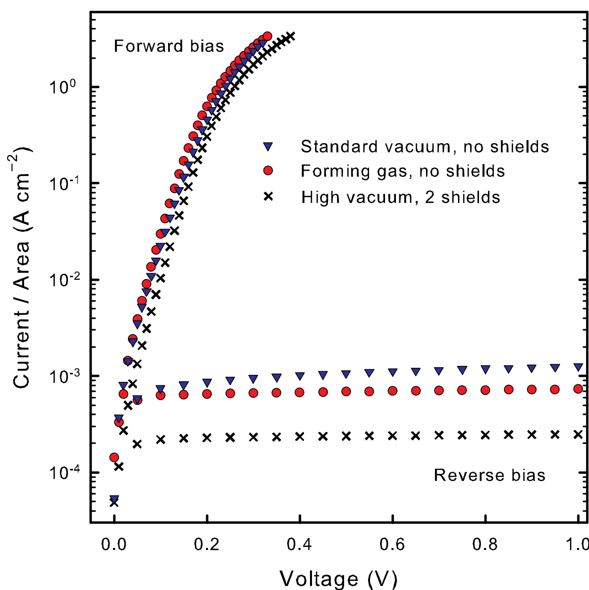

FIG. 4. Current vs voltage plots of Pt SBDs prepared by EBD in a vacuum that varies between 10^{-6} and 10^{-4} mbar without shielding (blue triangles); in forming gas at a pressure of 10^{-4} mbar (red circles) and with two shields at 10^{-6} mbar vacuum (crosses). Forward and reverse bias plots are displayed on the same positive x-axis.

C. Electron beam exposure, without deposition

In experimental setups, it is standard practice to mechanically shield samples until the evaporation has reached a stable state and the deposition is ready to proceed. This is not always practical in industrial systems where large areas have to be coated. An investigation of the effect of this practice was carried out by exposing samples to the conditions of EBD without deposition, termed EBE in this article. A beam with a current of 100 mA was rastered over a tungsten target as this did not produce evaporant from the target while still creating the conditions prevalent in the chamber during deposition of a lower melting point metal such as platinum.

Samples were exposed for 2, 10, or 50 min periods prior to RE of Pd Schottky barrier diodes onto the exposed surfaces. Subsequent DLTS scans revealed the presence of deep level defects in all samples in very low concentrations, and thus, only the 50 min EBE sample had defects in a high enough concentration to facilitate subsequent analysis (Figure 5). Pulse voltages applied were intentionally small to lower the effect that the electric field has on measurements. EBE followed by Pd RE was found to introduce an electron trap, $E_{0.16}$, as well as four hole traps, $H'_{0.15}$, $H_{0.22}$, $H_{0.26}$, and $H_{0.34}$. Characterization of these defects was performed using L-DLTS and is summarized in Table I. All these defects were found to be different from the EBD defects that were previously reported, as illustrated in the Arrhenius plot (Figure 6). While the Arrhenius plot of $H_{0.26}$ overlaps with the known $H_{0.30}$ defect with activation energy for hole emission from E(−/0) determined as 0.307 eV by Markevich *et al.*,[26] it is not likely to be the same defect as their apparent capture cross sections are different by a factor of 2. An annealing study will have to be performed in future as the final arbiter. By evaporating Au onto the EB exposed Ge surface, it was possible to obtain DLTS spectra where the electron-traps were dominant (DLTS—Figure 7 and Arrhenius plots—Figure 8). In plot (e) of Figure 7, five defects are visible: $E_{0.16}$, $E_{0.22}$, $H_{0.26}$, $E_{0.33}$, and $E_{0.38}$. L-DLTS further splits two of these peaks yielding the additional defects $E'_{0.22}$ and $E_{0.37}$. Only $E_{0.38}$ (E-center) and $E_{0.37}$ have been observed before. To the best of our knowledge, none of the other EBE-induced defects have been reported before. Defects $E_{0.16}$, $E_{0.22}$, and $E'_{0.22}$ annealed out within five days at room temperature, but the rest of the defects

[This article is copyrighted as indicated in the article. Reuse of AIP content is subject to the terms at: http://scitation.aip.org/termsconditions. Downloaded to] IP: 137.215.6.53 On: Tue, 22 Apr 2014 06:13:18

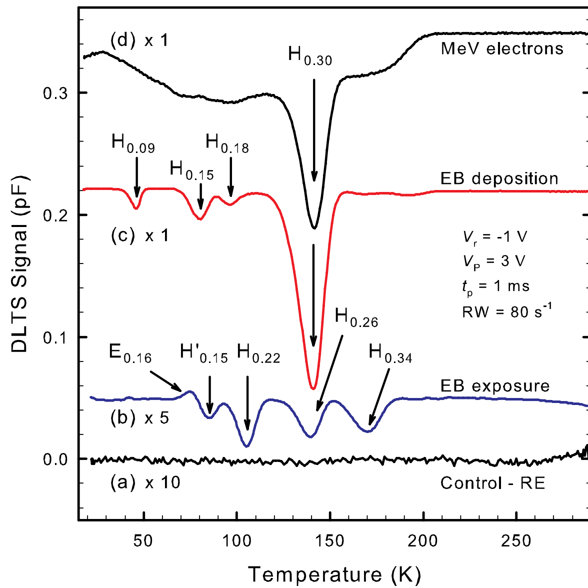

FIG. 5. An 80 s^{-1} rate window DLTS spectra recorded under hole-injection conditions for resistively evaporated Pd diodes where (a) is a RE control spectrum, (b) RE diode pre-exposed to EB conditions for 50 min, (c) EB deposited diode, and (d) a diode exposed to MeV electrons from a Sr-90 source.

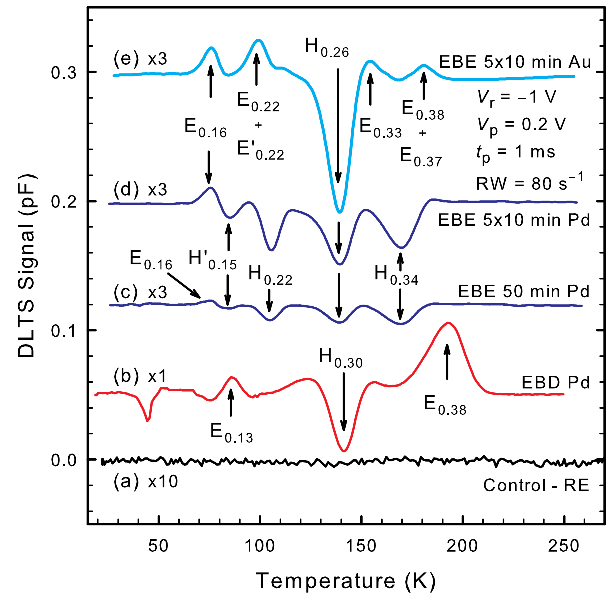

FIG. 7. 80 s^{-1} rate window DLTS spectra recorded at a reverse bias of 1 V, V_p of 0.2 V and pulse width of 1 ms for resistively evaporated diodes [(a), (c), (d), and (e)], where (a) is an Au control spectrum, (b) Pd EB deposited diode, (c) RE diode pre-exposed to EB conditions for 50 min, (d) a Pd RE diode RE pre-exposed to EB conditions for 5 × 10 minutes, and (e) a gold RE diode pre-exposed to EB conditions for 5 × 10 min.

remained almost unchanged. No further annealing studies have been undertaken.

By the end of a 50 min EBE treatment, the sample temperature had increased to approximately 365 K. Performing EBE in 10 min treatments with 50 min slots in between for cooling ensured that the sample temperature remained below 335 K. The effect of this strategy on defect concentration can be observed by comparing plots (c) and (d) of Figure 7. Peak heights were at least three times higher for all defects introduced by EBE in the cooler sample. Similar defect concentration changes were observed for the Au diodes.

IV. DISCUSSION

The significant differences between the DLTS spectra of the EBD and EBE diodes were surprising and not easily explained, especially as most of these defects have not yet been identified. With regards to the energy of impinging particles, the EBD samples were exposed to the lowest energy followed by EBE and 4 eV Ar ICP in order of increasing energy. In all these cases, particles with sub-threshold energy induced the observed defects, the difference being that in the EBD case energy was transferred to the sample through the metal contact,

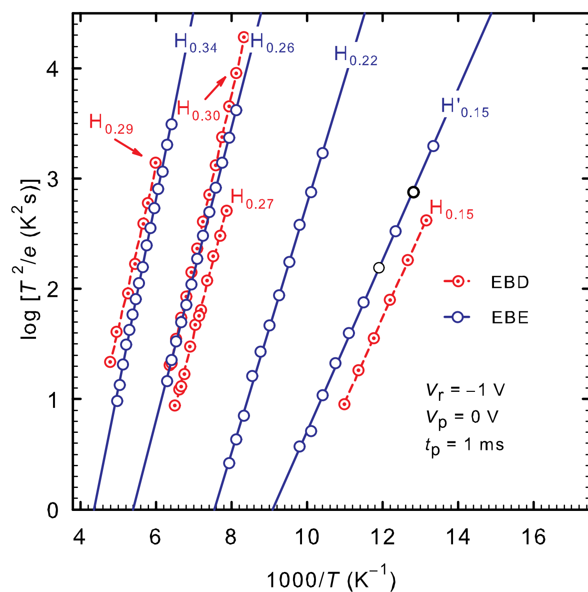

FIG. 6. Arrhenius plots of defects observed after EBD (red circles) and EBE followed by Pd evaporation (blue circles). Only empty circles that denote hole traps are shown as they dominate the Pd EBE spectrum. $E_{0.16}$ is plotted in Figure 8.

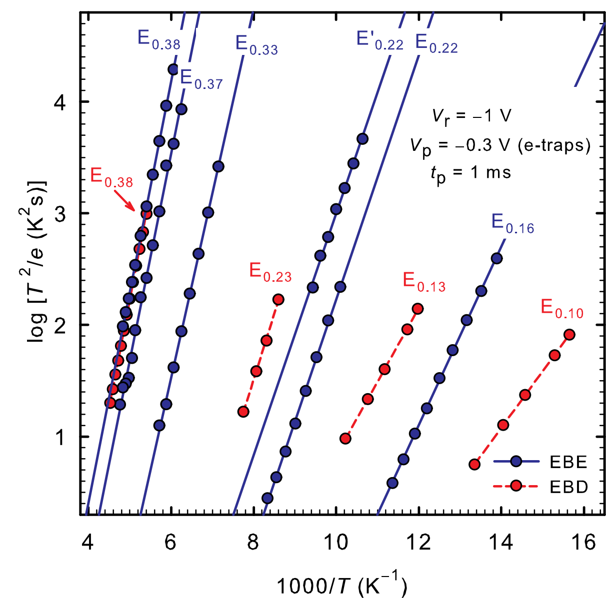

FIG. 8. Arrhenius plots of electron-trap defects observed after EBD (red circles) and EBE (blue circles). EBE defects were measured using Au diodes. Only EBD defects with similar energies to EBE defects are shown and the measurement parameters are noted in the figure.

[This article is copyrighted as indicated in the article. Reuse of AIP content is subject to the terms at: http://scitation.aip.org/termsconditions. Downloaded to] IP: 137.215.6.53 On: Tue, 22 Apr 2014 06:13:18

whereas in the EBE case, these energetic particles interact directly with the semiconductor surface. While it is unlikely that EBD-induced defects are the result of implantation, it is possible that some of the EBE-induced defects were caused by particles that were implanted during the EBE process and diffused deeper into the Ge. The presence of the E-center in EBD and EBE samples demonstrates that at least one defect is not implantation related. There was not enough energy available to generate Frenkel pairs in either of these processes, thus a mechanism to transfer energy deep into the Ge crystal was required to generate E-centers. Such a mechanism, known as discrete breathers (DBs), has been described theoretically and with experimental observations as well.[27] These stationary or moving non-linear localized lattice excitations, having energies in molecular dynamics (MD) from a few eV to 10 eV with long lifetimes, have been shown to exist in some metals.[28] Stationary breathers have been found in germanium[29] and work to demonstrate that moving breathers can also exist in this semiconductor, with a detailed analysis of the energy transfer from ion to crystal lattice will be published in a follow-up paper.

Phonon activity in the 50 min EBE sample disrupted defect introduction as the concentrations of all defects were lower than in the cooler sample. While it may be argued that defects in the sample exposed to a higher temperature annealed out, thus accounting for the lower concentrations observed, this small increase in temperature is highly unlikely to have affected all defects equally. EBE followed by Au RE yielded additional defects which is not observed in the Pd diodes, but a discussion of these differences is beyond the scope of this report.

V. CONCLUSIONS

Varying the conditions during EBD introduced two new defects, $E_{0.28}$ and $E_{0.31}$, which were not previously observed in Ge. The introduction of shields not only lowered defect concentrations but also ensured that superior diodes were produced. EBE that exposed the sample to very similar conditions as those of EBD was responsible for introducing ten defects. We can only speculate why the E-center and $E_{0.37}$ were the only defects that have previously been observed. To determine how sub-threshold particles cause damage in Ge, it was necessary to identify the energetic ions, atoms, or molecules generated in the electron beam path as the energy carriers, then consider the interaction of these energetic particles with light atoms in the crystal lattice, and subsequently identify a mechanism whereby energy can be transferred deep into the crystal without the need for an ion-solid interaction. As the shielded EBD samples continued to be bombarded by energetic electrons without significant damage being observed, it can be concluded that sub-threshold electrons are not responsible for the EBD-induced defects. The disruption of defect introduction by phonon activity in EBE diodes is further evidence that discrete breathers are the most likely energy transfer mechanism responsible for EBE as well as EBD-induced defects. As damage has been observed after EBD on Si and other semiconducting materials, it is safe to conclude that this damage causing mechanism is applicable to other semiconductors as well.

ACKNOWLEDGMENTS

The authors gratefully acknowledge financial support of the South African National Research Foundation. The Laplace DLTS software and hardware used in the research was kindly provided by A. R. Peaker (Centre for Electronic Materials Devices and Nanostructures, University of Manchester) and L. Dobaczewski (Institute of Physics, Polish Academy of Sciences). Special thanks to J. F. R. Archilla and D. I. Tetelbaum.

[1]E. Reinhold and J. Faber, Surf. Coat. Technol. **206**, 1653 (2011).
[2]S. Z. Karazhanov, J. Appl. Phys. **89**, 332 (2001).
[3]G. Myburg and F. D. Auret, J. Appl. Phys. **71**, 6172 (1992).
[4]Y. Chen and J. W. MacKay, Phys. Rev. **167**, 745 (1968).
[5]E. E. Haller, Mater. Sci. Semicond. Process. **9**, 408 (2006).
[6]F. D. Auret, S. M. M. Coelho, J. M. Nel, and W. E. Meyer, Phys. Status Solidi A **209**, 1926 (2012).
[7]L. Dobaczewski, P. Kaczor, I. D. Hawkins, and A. R. Peaker, J. Appl. Phys. **76**, 194 (1994).
[8]J. A. Lauber, S. Gascon-Shotkin, R. G. Kellogg, and G. R. Martinez, Nucl. Instrum. Methods Phys. Res. A **396**, 165 (1997).
[9]J. Fage-Pedersen, A. Nylandsted Larsen, and A. Mesli, Phys. Rev. B **62**, 10116 (2000).
[10]E. Holmstrom, K. Nordlund, and A. Kuronen, Phys. Scr. **81**, 035601(4 pages) (2010).
[11]P. M. Mooney and J. C. Bourgoin, Phys. Rev. B **29**, 1962 (1984).
[12]F. D. Auret, W. E. Meyer, S. Coelho, and M. Hayes, Appl. Phys. Lett. **88**, 242110 (2006).
[13]A. R. Peaker, V. P. Markevich, and L. Dobaczewski, *Defects in Microelectronic Materials and Devices* (CRC, New York, 2009), pp. 27–55.
[14]R. Jones, B. J. Coomer, J. P. Goss, B. Hourahine, and A. Resende, Solid State Phenom. **71**, 173 (2000).
[15]M. Budde, B. Bech Nielsen, P. Leary, J. Goss, R. Jones, P. Briddon, S. Öberg, and S. Breuer, Phys. Rev. B **57**, 4397 (1998).
[16]J. R. Weber, A. Janotti, P. Rinke, and C. G. Van de Walle, Appl. Phys. Lett. **91**, 142101 (2007).
[17]J. Weber, M. Hiller, and E. V. Lavrov, Mater. Sci. Semicond. Process. **9**, 564 (2006).
[18]B. J. F. Coomer, *A First Principles Study of Radiation Defects in Semiconductors* (University of Exeter, 2000).
[19]C. Kittel, *Introduction to Solid State Physics*, 6th ed. (Wiley, New York, 1986).
[20]*CRC Handbook of Chemistry and Physics*, 73rd ed., edited by David R. Lide (CRC Press, Boca Raton, FL, 1992).
[21]K. T. Roro, P. J. Janse van Rensburg, F. D. Auret, and S. Coelho, Physica B **404**, 4496 (2009).
[22]F. D. Auret, S. M. M. Coelho, G. Myburg, P. J. Janse van Rensburg, and W. E. Meyer, Physica B **404**, 4376 (2009).
[23]C. Nyamhere, A. Venter, D. M. Murape, F. D. Auret, S. M. M. Coelho, and J. R. Botha, Physica B **407**, 2935 (2012).
[24]C. Nyamhere, A. G. M. Das, F. D. Auret, A. Chawanda, W. Mtangi, Q. Odendaal, and A. Carr, Physica B **404**, 4379 (2009).
[25]F. D. Auret, W. E. Meyer, S. Coelho, M. Hayes, and J. M. Nel, Mater. Sci. Semicond. Process. **9**, 576 (2006).
[26]V. P. Markevich, I. D. Hawkins, A. R. Peaker, K. V. Emtsev, V. V. Emtsev, V. V. Litvinov, L. I. Murin, and L. Dobaczewski, Phys. Rev. B **70**, 235213 (2004).
[27]S. Flach and A. V. Gorbach, Phys. Rep. **467**, 1 (2008).
[28]V. Hizhnyakov, M. Haas, A. Pishtshev, A. Shelkan, and M. Klopov, Nuclear Instrum. Methods Phys. Res. B **303**, 91 (2013).
[29]N. K. Voulgarakis, G. Hadjisavvas, P. C. Kelires, and G. P. Tsironis, Phys. Rev. B **69**, 113201 (2004).
[30]V. P. Markevich, A. R. Peaker, V. V. Litvinov, V. V. Emtsev, and L. I. Murin, J. Appl. Phys. **95**, 4078 (2004).
[31]V. P. Markevich, Mater. Sci. Semicond. Process. **9**, 589 (2006).
[32]F. D. Auret, S. Coelho, W. E. Meyer, C. Nyamhere, M. Hayes, and J. M. Nel, J. Electron. Mater. **36**, 1604 (2007).
[33]C. Nyamhere, M. Das, F. D. Auret, and A. Chawanda, Phys. Status Solidi (C) **5**, 623 (2008).

[This article is copyrighted as indicated in the article. Reuse of AIP content is subject to the terms at: http://scitation.aip.org/termsconditions. Downloaded to] IP: 137.215.6.53 On: Tue, 22 Apr 2014 06:13:18